Desalination and Water Treatment
www.deswater.com
doi: 10.1080/19443994.2012.750585

51 (2013) 4684–4693
June

Taylor & Francis
Taylor & Francis Group

Numerical investigation for the supersonic steam jetting flow in the thermal vapor compressor

Yong Yang, Shengqiang Shen*, Shihe Zhou, Rui Liu, Huan Yu

Key Laboratry of Liaoning Province for Desalination, School of Power and Engineering, Dalian University of Technology, Dalian 116024, China
Tel. +86 411 84709822; Fax: +86 411 84707963; email: zzbshen@dlut.edu.cn

Received 27 September 2012; Accepted 8 November 2012

ABSTRACT

The thermal vapor compressor (TVC) is an essential part that governs the overall process in the multiple-effect distillation—TVC system. The supersonic steam jetting flow always occurs in the TVC equipment, and the flow in the TVC is very complex due to the strong compressibility, non-equilibrium phase change, and supersonic turbulent flow of the stream. So, to improve the performance of an ejector system, an investigation of the characteristics for the high speed flow inside the ejector is often required. In the present study, the supersonic steam jetting flow with non-equilibrium phase change and condensation shock was numerically studied based on the computational fluid dynamics method. A conservative compressible numerical model coupling with non-isothermal classical nucleation model and droplet growth model, in which the thermodynamic state and properties of steam was calculated by the Virial Equations, was developed and used to predict the supersonic non-equilibrium jetting flow. The effects of various operating pressures on the nozzle performance were investigated. The research explored the effect of steam pressure, temperature, supercooling level, and super-saturation ratio on the onset of the nucleation and the intensity of condensation shock in the supersonic steam flow.

Keywords: Thermal vapor compressor; Supersonic jetting flow; Shock; CFD

1. Introduction

Nucleation and condensation of steam always occurs in several natural and industrial processes including cloud formation, flight of aircraft in humid condition, power generation equipment, turbomechanical flow, and so on. With the expansion of the desalination industry [1,2], multiple-effect distillation (MED) with thermal vapor compressor (TVC) system becomes more attractive than other thermal systems due to effectiveness, easier operation and maintenance, and good economic characteristics, so MED–TVC desalination technology is taking a considerable portion in the desalination field, and the market size is growing rapidly especially in china [3–5]. The MED desalination plant is normally built in a dual-purpose power plant with electricity and fresh water production to increase the economy and thermal efficiency. In this case, the heating steam for the MED desalination plant is extracted from steam turbine, while the steam is normally with much higher pressure and temperature than the steam inducted into the desalination plant. Thus, to increase the energy utilization efficiency, the TVC device is usually used to make the vapor recycle as the pressure reducer. Since the performance of a TVC is affected obviously by the

*Corresponding author.

pressures of entrained vapor and motive steam, thus the thermodynamic state of the heating steam and the position of TVC in a MED desalination plant will affect its performance significantly. Therefore, the heating steam parameters, and the TVC suction position and its performance, are concerned by both academic researchers and engineers.

A schematic diagram of the MED–TVC desalination system is shown in Fig. 1 [6]. It includes mainly evaporators, a TVC device, and an end condenser. Other auxiliary equipments include distillate flashing boxes, brine flashing boxes, a venting system, sea water feeding, and brine and distillate expelling facilities. The TVC is an essential part that governs the overall process in the MED system. Accurate prediction of the TVC performance promotes the reliability of the process, increases the TVC entraining efficiency, and thus improves the performance of MED significantly. The flow and heat transfer in the TVC is very complex due to the strong compressibility, non-equilibrium phase change, and supersonic turbulent flow of the stream. Thus, studying the shock structure of the supersonic jets, visualizing the turbulent structures of the flow in the ejectors, and understanding the non-equilibrium phase change in the transonic steam flow are very important for predicting, and possibly controlling, when the resulting flow phenomena occur in the TVC system [7,8]. The current research focuses on the investigation of the spontaneous condensation and the condensation shocks in the rapid expansions in the TVC system.

As shown in Fig. 2, a typical TVC construction comprises four distinct parts: a convergent divergent nozzle, a suction chamber, a mixing chamber attached to a constant area duct, and a diffuser. The typical processes inside an ejector begin with high temperature and high pressure stream from the generator, entering the ejector through the convergent divergent nozzle. This stream is accelerated and expanded to supersonic speed at the nozzle exit where it creates an aerodynamic duct to entrain the low pressure and low temperature secondary stream into the mixing chamber. The secondary stream is accelerated to sonic velocity and mixes with the primary stream in the constant area duct. The region of supersonic flow is terminated by a normal shock wave further down the duct or in the diffuser [9]. In practice, two choking phenomena exist in the ejector performance [10], one in the primary flow through the nozzle and the other in the entrained flow. In addition to the choking in the nozzle, the second choking of an ejector results in the acceleration of the entrained flow from a stagnant state at the suction port to a supersonic flow in the constant-area section.

The entrainment ratio (ω, the ratio of mass flow rate of secondary fluid to that of primary fluid) is affected by many factors. The physical phenomena involve supersonic flow, shock interactions, and turbulent mixing of two streams inside the ejector enclosure. It is so complicated that the design of an ejector to date still heavily relies on trials and errors methods although a number of gas-dynamic theories for ejector analysis were developed by several researchers. Fig. 3 gives the typical performance curve for a fixed structure TVC [11]. The flow in the TVC device is usually in three modes: critical mode (with choking flow in

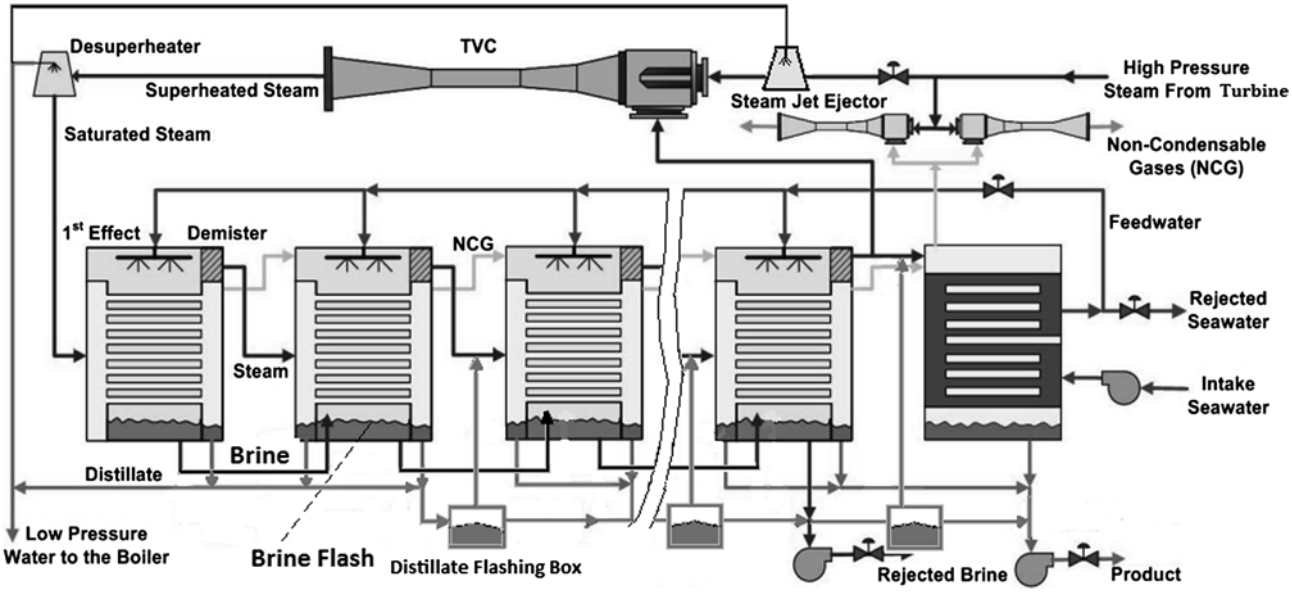

Fig. 1. Schematic diagram of MED–TVC system [6].

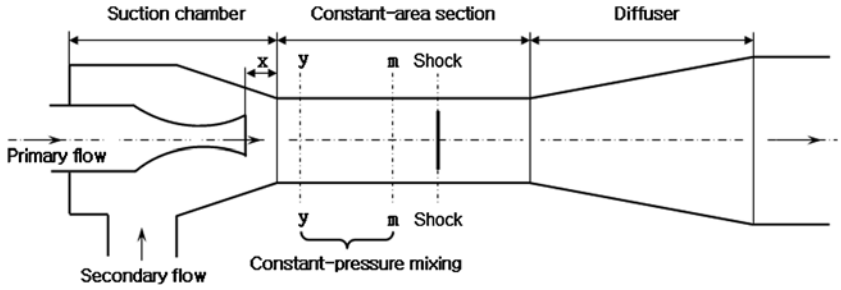

Fig. 2. Schematic diagram of the TVC construction.

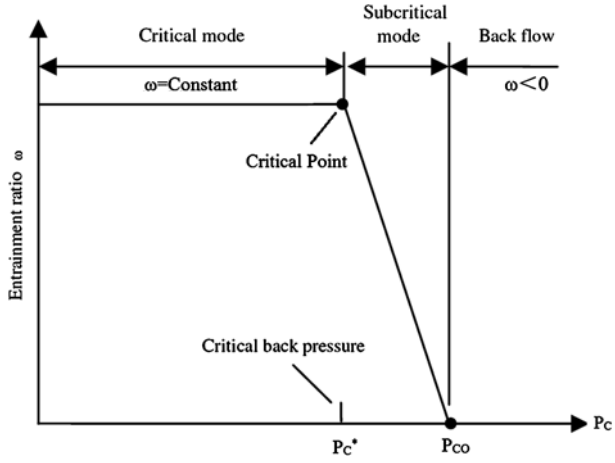

Fig. 3. Entrainment ratio as a function of discharge pressure P_c [11].

the mixing chamber), subcritical mode (without choking flow in the mixing chamber), and malfunction mode (with reversed flow in the mixing chamber) depended on different back pressure (P_C, discharge pressure of TVC). When P_C is below the critical value (P_C^*), the entrainment ratio remains constant. When P_C is increased higher than P_C^*, the entrainment ratio begins to fall down rapidly. A TVC should be operated at the critical mode to keep steady pumping performances, so it is very important to obtain the pumping performance curve, especially the critical point accurately in theoretical analysis and engineering applications.

In the TVC system, the working characteristic of the TVC has great impact on the system performance, and a slight change of the inlet or back pressure will cause great change for the TVC entraining efficiency. For example, a minor change of the suction pressure can lead to a drastic change on the TVC operating performance and the increase of the motive steam pressure can slightly improve the performance of the TVC under a certain range [12,13]. And in the case of steam expanding rapidly in the primary nozzle, condensation will occur in the form of homogenous nucleation after a high supersaturated state is attained. In such situation, the steam flow will be affected by the latent heat released from the condensation of vapor and the "condensation shocks" will occur in the type of pressure raise. In some early research, it is indicated that the pressure has great effect on the condensation in a supersonic nozzle [14]. So, exploring the effect of steam pressure on the onset of the nucleation and the intensity of condensation shock is an urgent research task.

To improve the performance of TVC and to investigate the characteristics for the heat transfer and high speed flow-in inside the nozzle in the TVC system, The present study reveals the pressure characteristics of the supersonic steam flow with homogenous nucleation and the condensation shocks in the nozzle. The supersonic steam flow with non-equilibrium phase change and condensation shock was numerically studied based on the computational fluid dynamics (CFD) method. And the special phenomena in the supersonic steam flow in the nozzle were investigated. The effects of various operating pressures and temperatures on the nozzle performance were investigated.

2. Mathematical model

2.1. Governing equations for the two-phase mixture

In this paper, a conservative two-dimensional compressible numerical model is developed under Eulerain coordinate system. The numerical simulation for the prediction of the non-equilibrium steam flow with spontaneous condensation in the conventional Laval nozzle is completed. To make the simulation availability and efficient, the condensing steam flow is assumed to be a mixture of steam and monodispersed droplets. That is, all droplets are of the same size at one point in the flow and the interactions between droplets are neglected. Since droplet sizes are

sufficiently small, it is assumed that the volume of the condensed liquid droplets is negligible and the velocity slip between the droplets and gaseous-phase is zero. And the density of the mixture is approximated as the following equation by neglecting the volume occupied by the liquid droplets,

$$\rho = \rho_g/(1-\beta) \tag{1}$$

where β is the overall mass fraction of the liquid phase.

Under the foregoing assumptions, the Euler equations may be written in integral form as follows:

$$\frac{\partial U}{\partial t} + \frac{\partial F}{\partial x} + \frac{\partial G}{\partial y} = 0 \tag{2}$$

where x, y, and t are the space and time coordinates and U, F, and G respectively defined as:

$$U = \begin{bmatrix} \rho \\ \rho u \\ \rho v \\ \rho E \end{bmatrix} F = \begin{bmatrix} \rho u \\ \rho u^2 + P \\ \rho uv \\ (\rho E + P)u \end{bmatrix} G = \begin{bmatrix} \rho v \\ \rho uv \\ \rho v^2 + P \\ (\rho E + P)v \end{bmatrix}$$

where P, u, v, E denote pressure, x-wise velocity, y-wise velocity, and internal energy, respectively. And the internal energy and specific enthalpy are determined as follows:

$$E = h_0 - P/\rho \tag{3}$$

$$h_0 = h + (u^2 + v^2)/2 \tag{4}$$

$$h = (1-\beta)h_g + \beta h_l \tag{5}$$

where h_0, h_g, and h_l are the enthalpy for the stagnation state condition, the gas phase, and the condensed liquid phase, respectively.

To model wet steam, two additional transport equations are needed [15]. The first transport equation governs the mass fraction of the condensed liquid phase (β) and the other transport equation (η) determines the number of droplets per unit volume. The two equations are combined to the model in the following expression:

$$\frac{\partial \rho}{\partial t}\beta + \nabla(\rho \vec{v}\beta) = \Gamma \tag{6}$$

$$\frac{\partial \rho}{\partial t}\eta + \nabla(\rho \vec{v}\eta) = PI \tag{7}$$

where Γ is the mass generation rate due to condensation and evaporation and I is the nucleation rate. And the number of droplets per unit volume (η) is calculated as follows:

$$\eta = \frac{\beta}{(1-\beta)V_d(\rho_l/\rho_g)} \tag{8}$$

$$V_d = \frac{4}{3}\pi \bar{r}^3 \tag{9}$$

where ρ_l, V_d, and $\bar{r}$ denote the liquid density, the average droplet volume, and the average droplet radius, respectively.

2.2. Nucleation model and droplet growth model for nucleating particles

In the model, the classical homogeneous nucleation theory describes the formation of a liquid-phase in the form of droplets from a supersaturated phase in the absence of impurities or foreign particles, and the nucleation rate is given by:

$$I = \frac{q_c}{1+\theta}\left(\frac{\rho_v^2}{\rho_l}\right)\sqrt{\frac{2\pi \mathrm{RT}}{M_m^3 \pi}}\exp\left(-\frac{4\pi r_*^2 \sigma}{3K_b T}\right) \tag{10}$$

where q_c is the evaporation coefficient, K_b is the Boltzmann constant, M_m the is mass of one molecule, σ is the liquid surface tension, and θ is a non-isothermal correction factor which is given by the following relation:

$$\theta = \frac{2(\gamma-1)}{(\gamma+1)}\left(\frac{h_{lv}}{\mathrm{RT}}\right)\left(\frac{h_{lv}}{\mathrm{RT}} - 0.5\right) \tag{11}$$

where h_{lv} is the specific enthalpy of evaporation at pressure P and γ is the ratio of specific heat capacities.

Based on the nucleation model just described the quantity of droplets at a location in the continuous gas phase is known, and the rate at which these droplets grow can be derived on the basis of heat transfer conditions surrounding the droplet [16]. This energy transfer relation can be written as:

$$\frac{\partial \bar{r}}{\partial t} = \frac{P}{h_{lv}\rho_l\sqrt{2\pi \mathrm{RT}}}\,\frac{\gamma+1}{2\gamma}\,C_p(T_l - T) \tag{12}$$

where T_l is the liquid droplet temperature.

Based on the above theory, the mass generation rate Γ is given by the sum of mass increase due to

nucleation and also due to growth/demise of these droplets and therefore, Γ is written as:

$$\Gamma = \frac{4}{3}\pi\rho_l I r_*^3 + 4\pi\rho_l \eta I \bar{r}^2 \frac{\partial \bar{r}}{\partial t} \tag{13}$$

where r_* is the Kelvin–Helmholtz critical droplet radius, above which the droplet will grow and below which the droplet will evaporate. And r_* is given as follows:

$$r_* = \frac{2\sigma}{\rho_l \mathrm{R}\mathrm{T} L_n S} \tag{14}$$

where S is the supersaturation ratio defined as the ratio of vapor pressure to the equilibrium saturation pressure:

$$S = \frac{P}{P_{sat}(T)} \tag{15}$$

After considering the nucleation model and the droplet growth model, we can get the source terms for the mass, momentum, and energy exchange between the gas and liquid phases. As in the simulation, it is assumed that the velocity slip between the droplets and gaseous-phase is zero, so the momentum source between the two phases can be neglected.

The steam equation of state used in the study, which relates the pressure to the vapor density and the temperature, is given by

$$p = \rho_v \mathrm{R}\mathrm{T}(1 + B\rho_v + C\rho_v^2) \tag{16}$$

where B and C are the second and the third Virial coefficients.

3. Effect of inlet pressure on condensation shock

3.1. Numerical validation: comparison vs. experimental values

The following example describes an application of the present model to the converging–diverging nozzle for the non-equilibrium condensing steam flow. The geometries of the converging–diverging nozzle (Fig. 4) were taken to be the same as the Nozzle B used in the experiment of Moore et al. [17]. To retain the calculation speed advantage coming with the use of regular block-structure element, the multi-block technique was applied to make the concentration of grid density focused on the areas where significant phenomena was expected.

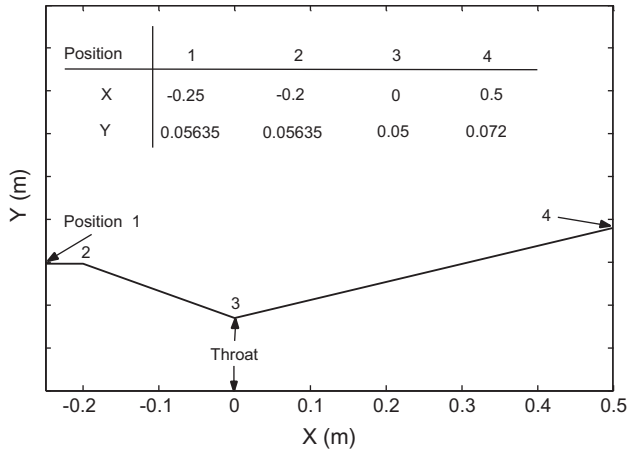

Fig. 4. Geometry of the nozzle.

The validation of the numerical results was accomplished with the experiment conducted by Moore [17] who obtained centerline pressure distributions for a series of converging–diverging nozzle configurations and the results showed a good agreement between numerical simulation and the experiment data. In Fig. 5 the pressure distribution along the centerline of the nozzle is compared with the experimental values for Nozzle B used in the experiment of Moore. As show in the Fig. 5, the profiles of the pressure distribution for the dry isentropic expansion and the non-equilibrium overlap before the location of the condensation shock where the pressure profile rises abruptly calculated by the non-equilibrium model. The simulation results are in good agreement with experiments for the converging–diverging nozzle before the location of the condensation shock, and the appearance of condensation shock is predicted accurately where a great amount of latent heat of condensate droplets is released causing an abrupt rise of pressure and temperature.

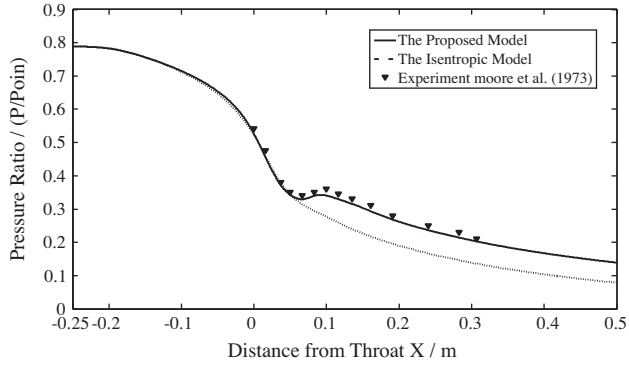

Fig. 5. Pressure distribution along the nozzle centerline compared with the experiment.

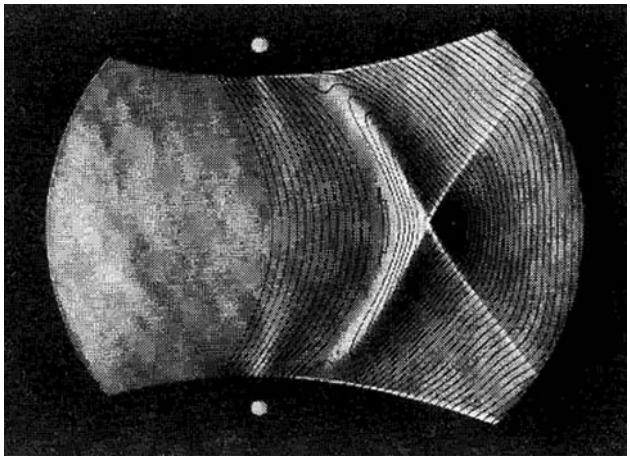

Fig. 6. Schlieren picture of condensation shock with Iso-Mach lines.

To validate the capability of the non-equilibrium model capture the condensation shock, another comparison has been made for the structure of the condensation shock. Fig. 6 shows a schlieren picture of a "Condensation shock" with Iso-Mach lines beginning at the sonic line [18]. The bright parabolic area corresponds to the continuous supersonic compression from the heat addition which creates the characteristic oblique shocks. Fig. 7 gives the structure of the calculated condensation shock with the Iso-Mach lines. The simulation result shows good agreement in the structure of the condensation shock with the schlieren picture.

3.2. Effect of inlet pressure on condensation shock

To investigate the effect of inlet parameters on the shock in the nozzle, the research explored the effect of steam pressure, temperature, supercooling level, and super-saturation ratio on the onset of the nucleation and the intensity of condensation shock in the supersonic steam flow.

The simulation results clearly show the process of the forming and weakening of condensation shock in the nozzle and the influence of the inlet pressure on the condensation shock. Fig. 8 gives the pressure profiles along the nozzle centerline for various inlet pressure values. Figs. 9–11, respectively, show the distribution of the temperature (T), the super saturation ratio (S), and the nucleation rate (I) along the centerline of the nozzle under the conditions with different inlet pressure values. And the numerical simulation

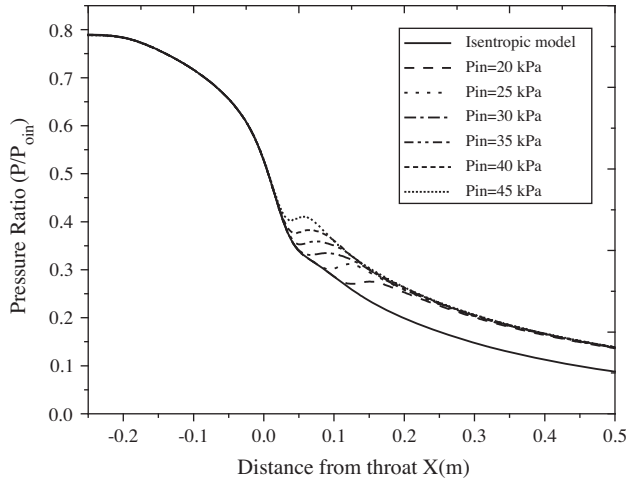

Fig. 8. Pressure profiles along the nozzle centerline for various inlet pressure.

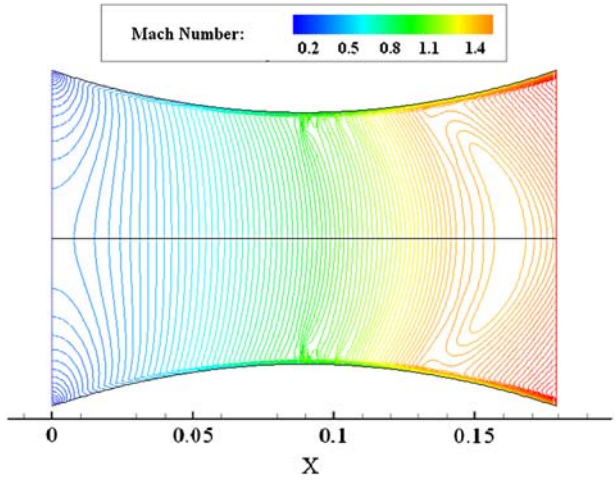

Fig. 7. Simulation result for the condensation chock with Iso-Mach Lines.

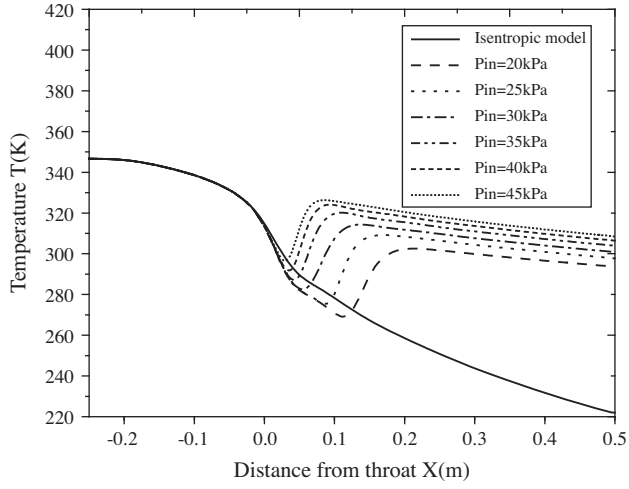

Fig. 9. Temperature profiles along the nozzle centerline for various inlet pressure.

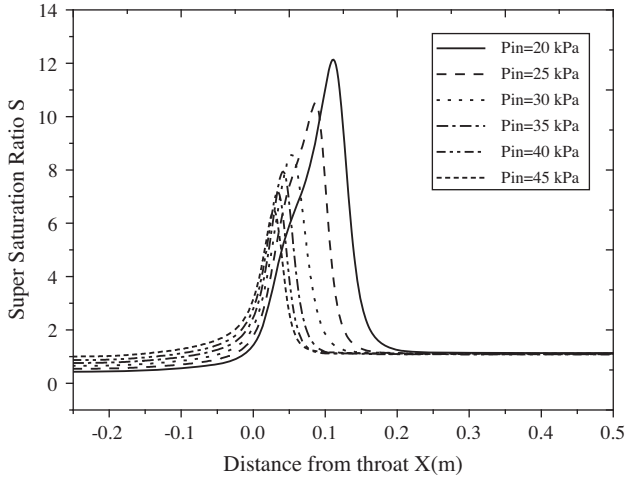

Fig. 10. Super saturation ratio profiles along the nozzle centerline for various inlet pressure.

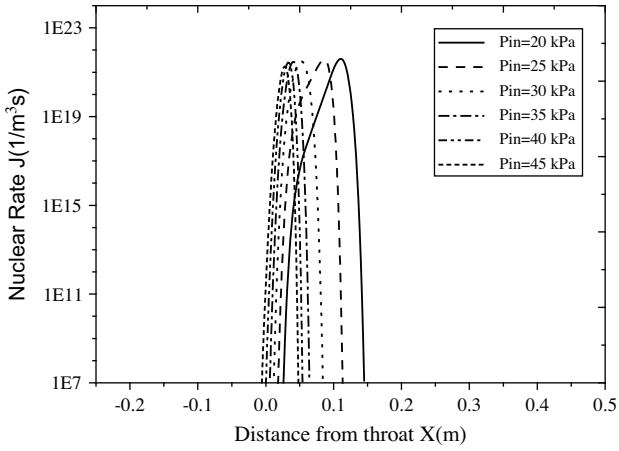

Fig. 11. Nucleation rate profiles along the nozzle centerline for various inlet pressure.

that used the proposed model has been compared with the dry isentropic expansion solution.

As shown in the figures, in the nozzle, the cross-sectional flow area first decreases to the throat and then increases monotonically in the supersonic region. As the steam flows through the nozzle, it expands and the temperature falls rapidly. Because the equilibrium vapor pressure decreases exponentially with temperature, very high supersaturation can be achieved. Eventually, the steam acquires sufficient supercooling for spontaneous nucleation of droplets in the diverging section of the nozzle, where the flow is supersonic. The subsequent release of latent heat thus results in a deceleration of the flow and a rise in pressure, known traditionally as the "condensation shock".

At the location of the condensation shock, a significant amount of liquid droplets generate, approximately 10^{21} droplets per second per unit volume (Fig. 11). And a sharp rise in wetness fraction achieves, reflecting the rapid growth of the droplets immediately following the peak nucleation. Referring again to Fig. 10, it is shown that after peak nucleation, the super saturation ratio rapidly drops to near equilibrium conditions ($s \approx 1$), where the supercooling level of the steam is lower than 5 K. This near equilibrium condition prevails in the remaining length of the nozzle for the supersonic outflow case.

As shown in Table 1 and Fig. 12, based on the comparison between the different conditions with several inlet pressure values ($P_{in} = 20$, 25, 30, 35, 40, and 45 kPa), the location of the condensation shock can be revealed clearly moving to the outlet of the nozzle from the throat (from 0.028 to 0.112 m) with the pressure becoming lower. And as shown in Fig. 12, when the inlet pressure decreases, the strength of the condensation shock is also weakened. Because at the same inlet temperature, the higher the inlet pressure is, the higher super saturation ratio the steam will achieves at the inlet of the nozzle. As shown in Fig. 9, when the steam is expanded in the converging–diverging nozzle,

Table 1
The main characteristics of the condensation chocks for different inlet pressures

Inlet pressure P (kPa)	Onset point of the condensation shock X (m)	Super saturation ratio of onset point (S)	Nucleation rate I of onset point I ($1/m^{-3}s^{-1}$)	Mach number of the onset point (Ma)
20	0.112	12.13	3.99×10^{21}	1.48
25	0.087	10.53	3.88×10^{21}	1.41
30	0.053	8.57	3.05×10^{21}	1.34
35	0.042	7.95	2.96×10^{21}	1.30
40	0.033	7.18	2.81×10^{21}	1.25
45	0.028	6.46	1.83×10^{21}	1.20

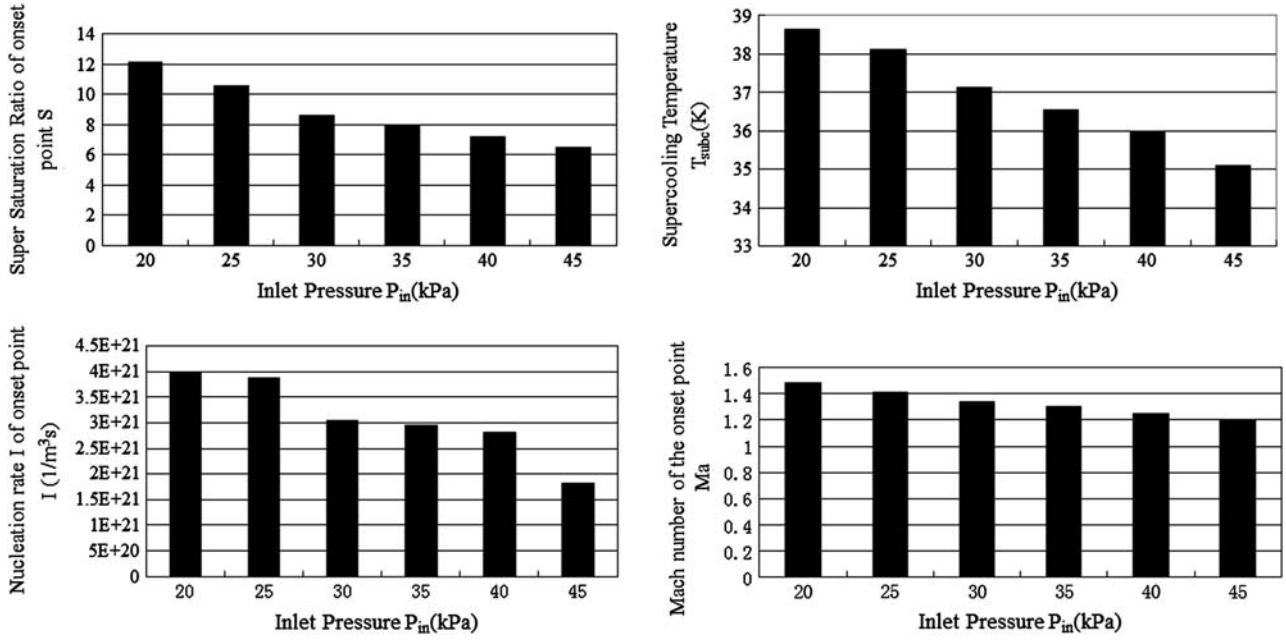

Fig. 12. Main characteristics of onset for condensation under different inlet pressures.

the temperature decreases rapidly to make the isentropic expansion vapor crosses the saturation line quickly and stays in a supersaturated state until the spontaneous condensation occurs suddenly where the ultimate supercooling achieves. As shown in Fig. 12, when the inlet pressure is higher, the ultimate supercooling achieves much easier after the throat and the droplet radius grows much larger and more rapidly, although the nucleation rate becomes a little smaller.

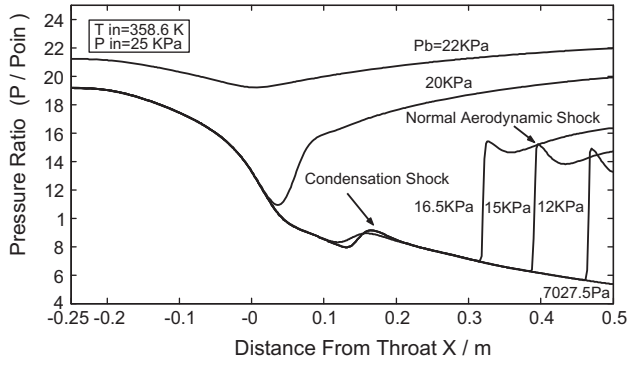

Fig. 13. Pressure distribution along the nozzle centerline for various back pressure.

4. Effect of back pressure on condensation shock

To examine the effect of the back pressure on the spontaneous condensation, for the same inlet boundary conditions at inflow ($P_{in} = 25$ kPa and $T_{oin} = 358.6$ K), a series of back pressures ($P_b = 7$, 12, 15, 16.5, 20, and 22 kPa) were obtained at the exit plane.

As is apparent in Figs. 13–15, when the out flow is supersonic ($P_b = 7$ kPa), the spontaneous homogenous nucleation and the condensation shock will appear as forecast. While in the case with a subsonic out flow ($P_b = 12$, 15, and 16.5 kPa), aerodynamic shock appears in the supersonic flow. The flow conditions upstream of the aerodynamic shock are the same as those for supersonic outflow case ($P_b = 7$ kPa). Through the aerodynamic shock, liquid droplets rapidly evaporate in response to the rapid pressure and temperature rise across the shock (Figs. 13 and 15). Downstream of the aerodynamic shock, the temperature falls abruptly due

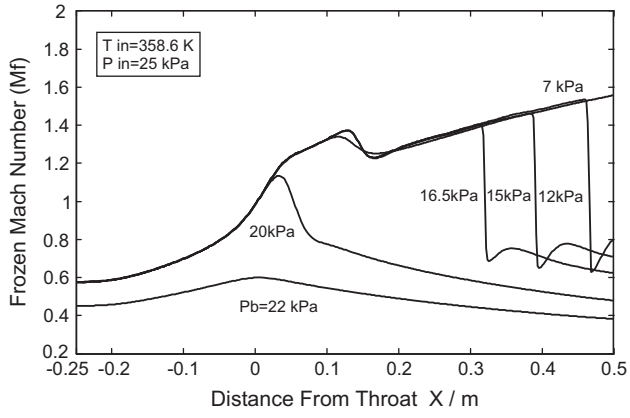

Fig. 14. Mach number distribution along the nozzle centerline for various back pressure.

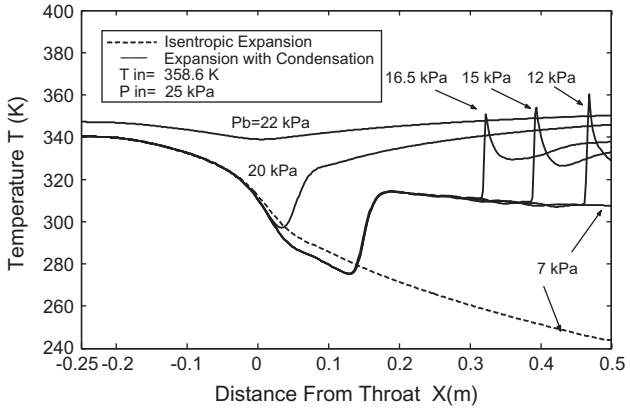

Fig. 15. Temperature distribution along the nozzle centerline for various back pressure.

to reacceleration of the flow and, after another peak point, the flow will decelerate with a small negative value of supercooling level to support heat movement toward the liquid phase as evaporation continues on droplet surfaces and wetness fraction reduces.

As shown in the figures, with the back pressure increases the normal aerodynamic shock moves toward the nozzle throat, and the strength of the aerodynamic shock decreases. If the normal aerodynamic shock passes through the location of the condensation shock ($P_b = 20$, 22 kPa), the spontaneous condensation will be weakened or even not occur at all. As the appearance of the aerodynamic shock will cause significant energy dissipation to make the steam flow decelerate to subsonic, the supercooling level achieves to only several degrees or even superheated conditions.

5. Conclusions

In the present study, the supersonic non-equilibrium steam flow with spontaneous condensation and condensation shock was numerically studied based on the CFD method. A conservative compressible numerical model coupling with non-isothermal classical nucleation model and droplet growth model was developed and used to predict the spontaneous condensation phenomenon with homogenous nucleation in the supersonic steam flow. The model has been validated against the experimental data and the results are in excellent agreement with experiments.

Based on the simulation, the effect of inlet pressure changing and outlet pressure changing on the thermodynamic and aerodynamic properties of condensation shock was studied. The research explored the effect of steam pressure, temperature, supercooling level, and super-saturation ratio on the onset of the nucleation and the intensity of condensation shock in the supersonic steam flow. And the main conclusions were obtained as follows:

(1) Different from the isentropic expansion, in supersonic steam flow non-equilibrium spontaneous condensation will occur in the form of "condensation shock" downstream of the nozzle throat, when the supercooling, and the super saturation ratio achieve a high level.
(2) The location of the condensation shock can be revealed, clearly moving to the outlet of the nozzle from the throat with the inlet pressure becoming lower. And when the inlet pressure decreases, the strength of the condensation shock is also weakened.
(3) With the back pressure increases the normal aerodynamic shock will appears, and the normal aerodynamic shock moves toward the nozzle throat. The aerodynamic shock has a complex influence on the homogeneous nucleation condensation. If the normal aerodynamic shock passes through the location of the condensation shock, the spontaneous condensation will be weakened or even not occur at all.

Nomencalture

B	—	the second Virial coefficient (m^3/kg)
C	—	the third Virial coefficient (m^6/kg^2)
C_p	—	specific heat capacity (J/kg K)
E	—	total specific internal energy (J/kg)
e	—	specific internal energy (J/kg)
h	—	static enthalpy (J/kg)
h_{lv}	—	specific enthalpy of evaporation (J/kg)
I	—	nucleation rate ($1/m^3$ s)
K_b	—	Boltzmann constant ($=1.3807 \times 10^{-23}$ J/K)
m	—	mass (kg)
P	—	pressure (Pa)
r	—	radius of droplets (m)
$\vec{r}$	—	mean droplet radius of droplets (m)
r_*	—	droplet critical radius (m)
S	—	super saturation ratio
T	—	temperature (K)
T_{subc}	—	supercooling level (K)
u	—	X-axial velocity (m/s)
v	—	Y-axial velocity (m/s)

Greek symbols

β	—	mass fraction of the condensed phase
γ	—	the ratio of specific heat capacities
Γ	—	mass generation rate (kg/m^3 s)
θ	—	nonisothermal correction factor
ρ	—	density (kg/m^3)
σ	—	liquid surface tension (N/m)

Subscripts

0	—	stagnation state condition
g	—	gas (vapor)
l	—	liquid

Superscripts

→	—	vector
—	—	average of a variable

Acknowledgments

This research is supported by the National Natural Science Foundation of China (No. 51206015) and the Postdoctoral Science Foundation of China (2012T50253).

References

[1] L.P. Yang, S.Q. Shen, Assessment of energy requirement for water production at dual-purpose plants in China, Desalination 205(1–3) (2007) 214–223.
[2] R. Kouhikamali, N. Sharifi, Experience of modification of thermo-compressors in multiple effects desalination plants in Assaluyeh in IRAN, Appl. Therm. Eng. 40 (2012) 174–180.
[3] R.K. Kamali, A. Abbassi, S.A. Sadough Vanini, A simulation model and parametric study of MED–TVC process, Desalination 235(1–3) (2009) 340–351.
[4] H.S. Choi, Y.G. Kim, S.L. Song, Performance improvement of multiple-effect distiller with thermal vapor compression system by energy analysis, Desalination 182(1–3) (2005) 239–249.
[5] M.A. Sharaf, A.S. Nafey, L. García-Rodríguez, Thermo-economic analysis of solar thermal power cycles assisted MED-VC (multi effect distillation-vapor compression) desalination processes, Energy 36(5) (2011) 2753–2764.
[6] M. Ameri, S.S. Mohammadi, M. Hosseini, M. Seifi, Effect of design parameters on multi-effect desalination system specifications[J], Desalination 245 (2009) 266–283.
[7] M.K. Ji, T. Utomo, J.S. Woo, Y.H. Lee, H.M. Jeong, H.S. Chung, CFD investigation on the flow structure inside thermo vapor compressor, Energy 35(6) (2010) 2694–2702.
[8] P. Desevaux, A. Mellal, Y. Alves de Sousa, Visualization of secondary flow choking phenomena in a supersonic air ejector, J. Visual. 7 (2004) 249–256.
[9] D.W. Sun, Comparative study of the performance of an ejector refrigeration cycle operating with various refrigerants, Energy Convers. Manage. 40(8) (1999) 873–884.
[10] J.T. Munday, D.F. Bagster, A new ejector theory applied to steam jet refrigeration, Ind. Chem. Process. Des. Del. 16(4) (1977) 442–449.
[11] B.J. Huang, J.M. Chang, C.P. Wang et al., A 1-d analysis of ejector performance, Int. J. Refrig. 22 (1999) 354–364.
[12] J.G. Ji, L.X. Li, R.Z. Wang, Performance simulation and analysis of steam ejector under different operating condition, Chem. Eng. 35(2) (2007) 68–71.
[13] J.G. Ji, R.Z. Wang, L.X. Li, Performance computation and analysis of steam ejector, Ship Eng. 28(5) (2006) 46–49.
[14] M.J. Kermani, A.G. Gerber, A general formula for the evaluation of thermodynamic and aerodynamic losses in nucleating steam flow, Int. J. Heat Mass Transfer. 46 (2003) 3265–3278.
[15] K. Ishazaki, T. Ikohagi, H. Daiguji, A high-resolution numerical method for transonic non-equilibrium condensation flows through a steam turbine cascade, Proceeding of the Sixth International Symposium on Computational Fluid Dynamics, Lake Tahoe, Nevada, USA, 1995, p. 479–484.
[16] J.B. Young, The spontaneous condensation of steam in supersonic nozzles, Phys. Chem. Hydrodyn. 3(2) (1982) 57–82.
[17] M.J. Moore, P.T. Walters, R.I. Crane, B.J. Davidson, Predicting the fog drop size in wet steam turbines, Wet Steam Fourth Conference, Institution of Mechanical Engineers, Coventry, UK, 1973, p. 101–109.
[18] G.H. Schnerr, R. Bohning, Compressible turbulent boundary layers with heat addition by homogeneous condensation, AIAA J. 30(5) (1992) 1284–1289.